

# Structural and electronic properties of coiled and curled carbon nanotubes having a large number of pentagon–heptagon pairs

Ph. Lambin

*Département de Physique, Facultés Universitaires Notre Dame de la Paix, 61 Rue de Bruxelles, B 5000 Namur, Belgium*

G. I. Márk and L. P. Biró

*Research Institute for Technical Physics and Materials Science, P.O. Box 49, H-1525 Budapest, Hungary*

(Received 2 December 2002; revised manuscript received 6 March 2003; published 16 May 2003)

A family of Haeckelite nanotubes is generated by rolling up a two-dimensional threefold coordinated carbon network composed of pentagon-heptagon pairs and hexagons in proportion 2:3. The corresponding two-dimensional network is highly strained due to the presence of adjacent pentagons and heptagons. When the sheet is folded into a cylinder, part of the strain is released by having the pentagons protrude outward, and sometimes inward the tube. Due to that property, a large variety of structures can be generated such as coiled, screwlike, curled, and pearl-necklace-like nanotubes. All the Haeckelite nanotubes obtained in this work are semiconductors, some having a small band gap. Scanning-tunneling microscopy images, computed for a few Haeckelite nanotubes, show salient topographic protrusions at the location of the pentagon pairs.

DOI: 10.1103/PhysRevB.67.205413

PACS number(s): 61.46.+w, 68.37.Ef, 45.10.Db, 81.15.Gh

## I. INTRODUCTION

Carbon is a remarkable element that shows a variety of stable structures ranging from three-dimensional (3D) diamond to 0D fullerenes through 2D graphite and 1D nanotubes. These different forms are the consequence of the several possible electronic configurations of carbon. The recent discovery that fullerenes and nanotubes can form spontaneously under special but quite versatile conditions has been followed by the observation that graphitic carbon can adopt many types of curvatures. Depending on the preparation techniques and conditions, different kinds of structures have been revealed by high-resolution transmission-electron microscopy (HRTEM), scanning-tunneling microscopy (STM) and atomic force microscopy, such as carbon onions,<sup>1</sup> tripods,<sup>2</sup> helices,<sup>3</sup> rings<sup>4</sup> and tori,<sup>5</sup> disks and cones,<sup>6</sup> nanohorns,<sup>7</sup> and Y-branched tubes.<sup>8–10</sup> Most of these structures can be explained if one incorporates pentagons and heptagons or larger polygons in the carbon honeycomb network.<sup>11</sup>

Pentagons are certainly present in fullerenes, nanotube caps,<sup>12</sup> and nanocones.<sup>6</sup> The presence of heptagons is suspected in some negatively curved parts of multiwall nanotubes,<sup>12,13</sup> in ideal Y-type tube connections,<sup>14</sup> and more in sophisticated nanotube junctions.<sup>15</sup> Pentagons and heptagons are very often grouped in pairs<sup>16</sup> or in the form of Stone-Wales defects which are associations of two such pairs. A systematic atomic resolution study of single-wall carbon nanotubes grown by laser ablation revealed that about 10% of the nanotubes show intramolecular junctions, i.e., localized defects which may change the chirality of the structure and have a clear signature in STM.<sup>17</sup> In the topographic STM images of these regions, the altered electronic structure due to the defects dominates over the atomic structure. Atomic models in which fused heptagon-pentagon pairs were incorporated in combination with tight-binding calculations made it possible to identify possible defect structures based

on measured and calculated scanning-tunneling spectroscopy (STS) data.

The presence of pentagon–heptagon pairs, and more specifically Stone-Wales defects, in nanotubes is highly suspected, perhaps at a part per hundred level,<sup>18</sup> although no direct observation can confirm this. In direct connection with this high concentration of defects, a large quantity of pentagons and heptagons is actually required in ideal helical coiled nanotubes to bend the structure.<sup>19</sup> In fact, helical structures can be produced at high yield by catalytic chemical vapor deposition (CVD).<sup>3,20</sup> Recently, the production of double- and triple-strand coiled carbon nanotubes was reported too.<sup>21</sup> The problem is to explain how pentagons and heptagons can be incorporated regularly in the structure during the nanotube growth process in order to generate a regular pitch and diameter of the helix.

As an alternative to the periodic insertion of pentagons and heptagons in the honeycomb network, László and Rassat have proposed to start with planar patterns of azulene units, which are fused pentagon-heptagon pairs.<sup>22</sup> Rolling up a stripe of azulenes, possibly mixed with hexagons, leads to a tube that automatically bends and may close itself in a torus.<sup>23,24</sup> This construction resembles the one used to generate Haeckelite nanotubes, which contain roughly equal numbers of pentagons, hexagons, and heptagons, but remain straight cylinders.<sup>25</sup> Recently, Biró *et al.* applied the idea of László and Rassat by assembling more complex patterns of azulenes and hexagons, and showed that specific wrappings of these structures lead to a new variety of toroidal, coiled, screwlike, and pearl-necklace-like structures.<sup>26</sup> The coiling appears naturally by rolling up a Haeckelite-like stripe and does not demand the insertion of additional polygons. The building blocks are azulene and hexagonal units in proportions that can vary from 2:1 to 2:3. In the coiled nanotubes produced by CVD, it is not impossible that such a high concentration of azulene units in the structure is the result of a fast kinetic that leads to metastable states due to the low growth temperature.

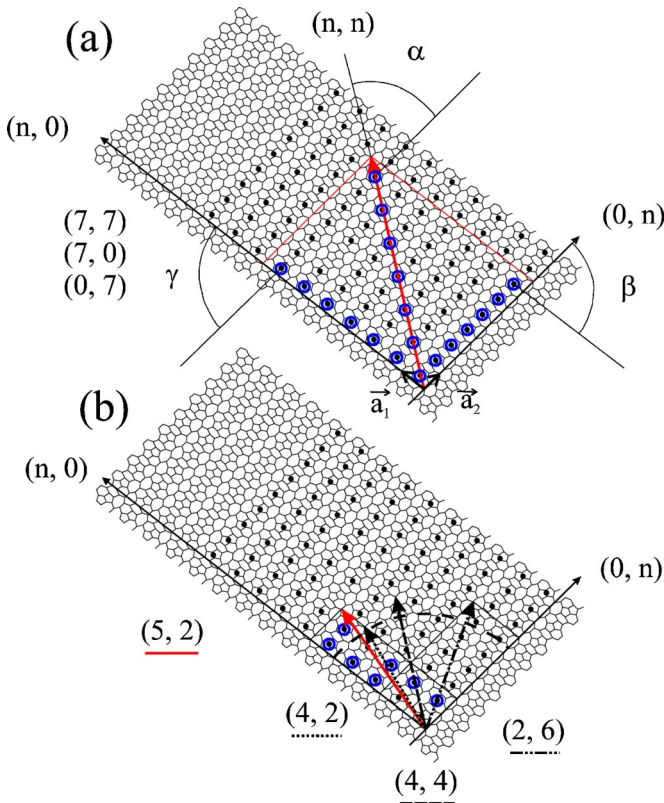


FIG. 1. (Color online) Regular tiling of the plane with hexagons and azulene units in proportion 3:2. The unit cell is defined by the primitive vectors  $\vec{a}_1$  and  $\vec{a}_2$ . The bonds shared by two pentagons (“stressors”) have been highlighted by black dots. In (a), a  $7 \times 7$  cell is shown to illustrate the wrapping vectors  $(7,0)$ ,  $(0,7)$ , and  $(7,7)$  along the special directions  $(n,0)$ ,  $(0,n)$ , and  $(n,n)$ . The stressors closest to the wrapping vectors are encircled. Rows of stressors are indicated by the thin solid lines defining the angles  $\alpha$ ,  $\beta$ , and  $\gamma$ . These rows will generate helical patterns along the structure. In (b), the wrapping vectors  $(4,2)$ ,  $(5,2)$ ,  $(4,4)$ , and  $(2,6)$  are represented by arrows. The asymmetrically placed stressors in the unit cell  $(5,2)$  are highlighted by encircling. In the unit cell  $(2,6)$ , all stressors are symmetrically placed around the wrapping vector. The dashed-line circle corresponds to a critical nanotube radius of 0.45 nm above which some stressors can dip inward toward the structure (see text).

## II. STRUCTURAL PROPERTIES

The structures were generated by rolling up a perfect, threefold coordinated carbon network as shown in Fig. 1. This network is a periodic tiling made of azulene units (5–7 pairs) and hexagons generated by placing  $57\text{-}3 \times 6$  unit cells side by side, described in detail earlier.<sup>26</sup> This kind of stripe is built of three hexagons and two azulene units (at the ends) per unit cell, which contains 14 atoms. The hexagons are not regular because the structure was optimized in the plane with periodic boundary conditions. The primitive vectors of the structure  $\vec{a}_1$  and  $\vec{a}_2$  have lengths of 0.700 and 0.522 nm, respectively, and the angle between them is  $97.8^\circ$ .

Stripes of the Haeckelite-like 2D network shown in Fig. 1 were rolled up following the usual wrapping rules used for graphitic nanotubes. In this construction, the site at the origin of the primitive vectors  $\vec{a}_1$  and  $\vec{a}_2$  is superimposed on the

TABLE I. List of Haeckelite nanotubes that were generated from the planar network shown in Fig. 1. Wrapping indices are  $(n,m)$ , initial diameter  $d = C_h/\pi$ , energy per atom is  $\Delta E$ , and width of the topological band gap is  $E_g$ .

$(n,m)$	$d$ (nm)	$\Delta E$ (eV/atom)	$E_g$ (eV)
(1,0)	0.223	−6.38	
(2,0)	0.446	−6.81	
(3,0)	0.669	−6.92	0.67
(4,0)	0.892	−7.00	~0.1
(1,1)	0.259	−6.69	
(2,2)	0.519	−6.96	
(3,3)	0.778	−6.98	0.57
(4,4)	1.038	−7.04	0.48
(0,4)	0.665	−7.06	0.65
(3,2)	0.705	−6.93	0.76
(2,6)	1.036	−7.08	0.40
(5,2)	1.119	−7.02	~0.1

site located at  $\vec{C}_h = n\vec{a}_1 + m\vec{a}_2$  and the tube  $(n,m)$  is obtained. The length of the rolled-up structures corresponded to 10 to 15 units along the  $\vec{a}_2$  vector when  $n \geq m$ , or 8 to 12 units along the  $\vec{a}_1$  vector in the other cases. The atomic structure of the perfectly cylindrical nanotube so generated was then fully relaxed with a conjugate-gradient algorithm, using the Brenner-Tersoff potential. The energy of the optimized structures listed in Table I is the average energy of the three-fold coordinated atoms. In such a way, the effects of the open ends are partly eliminated.

The network shown in Fig. 1, in a similar way to the graphene sheet in the case of rolling up straight carbon nanotubes,<sup>27</sup> possesses a number of particular rolling directions: the two axes  $(n,0)$  and  $(0,n)$ , and the line  $(n,n)$ . On the other hand due to the much lower symmetry of the network than that for graphene, all the points with  $(n > 0, m)$  define individual structures. The  $(0,0)$  point also has some peculiarities. It is close to constituting an inversion center for structures which can be generated so that all the structures  $(n > 0, m)$  will have an almost structurally identical correspondent in the half plane for which  $n < 0$ . Due to the fact that the origin of the axes is fixed at one apex of a heptagon, it cannot be a real inversion center, still the objects defined by  $(n,m)$  and  $(-n,-m)$  will have structures very close to each other.

In Fig. 1 the common bond of the two adjacent pentagons was highlighted by heavy dots, because in all the tubular structures generated, this bond was found to be a stress concentrator placed in regions with strong local curvature. These bonds will be called from here on *stressors*. The unit cell defined by  $(1,1)$  contains one such stressor. The stressors will generate regions of protruding (positive stressor) or dipping (negative stressor) local curvature, which will spiral along the tube. In Fig. 1(a) the distribution of the stressors around the circumference of three tubular structures  $(7,7)$ ,  $(7,0)$ , and  $(0,7)$  have been further highlighted by encircling. These will be used to discuss the three particular directions mentioned above. As in the case of nanotubes generated from graphene,

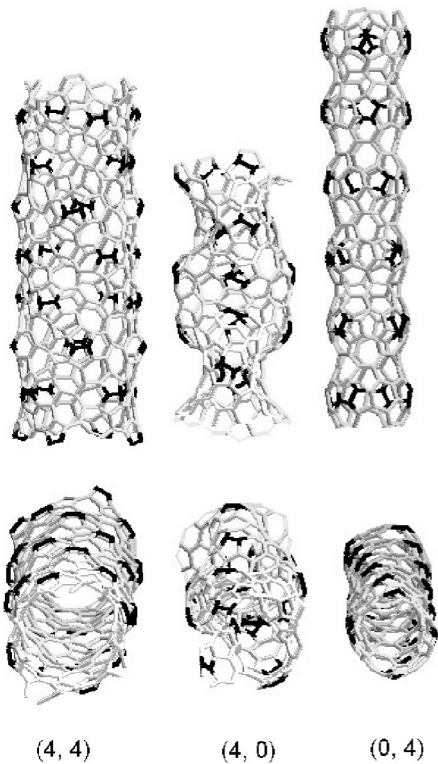


FIG. 2. Atomic structures of open-end nanotubes with indices (4,4), (4,0), and (0,4) viewed from a direction perpendicular to the axis (top) or close to the axis (bottom).

the wrapping vector will become a closed curve (not necessarily a circle in the case of small  $n$ ) on the tubular structure, which defines a plane locally perpendicular to the tube axis even in the case of more complex shapes. The safest way to decide the number of stressor stripes spiraling along the circumference of a tubular structure is to count the number of highlighted heavy dots closest to the wrapping vector. As discussed later on in this section, it may happen that not all stressors will generate protrusions, in which case the surface will be curved locally in such a way that the continuity of the stripe generated by the spiraling positive stressor is maintained. In this way, one can easily observe that the number of such stripes, called the “multiplicity” of the tubular structure, will be seven for all the structures discussed in this paragraph. The angles under which these seven rows of protrusions are seen from the wrapping vector is different for each of the (7,7), (7,0), and (0,7) structures. This means that the pitch of the multiple helices will be different for each tube. In order to save computing capacity the three discussed notable directions are illustrated for  $n=4$ . The structures were generated as described above.

In Fig. 2 the views close to the axial (viewing along the axis) and the longitudinal views (viewing perpendicular to the axis) are shown for the tubular structures (4,4), (4,0), and (0,4). One may notice that for all the structures, even for the very “crumpled” (4,0), there is either zero or a multiple of four stressors in any section of the tubular structure, provided the borders of the section are chosen normal to the tube axis. Another common feature is that in the axial views

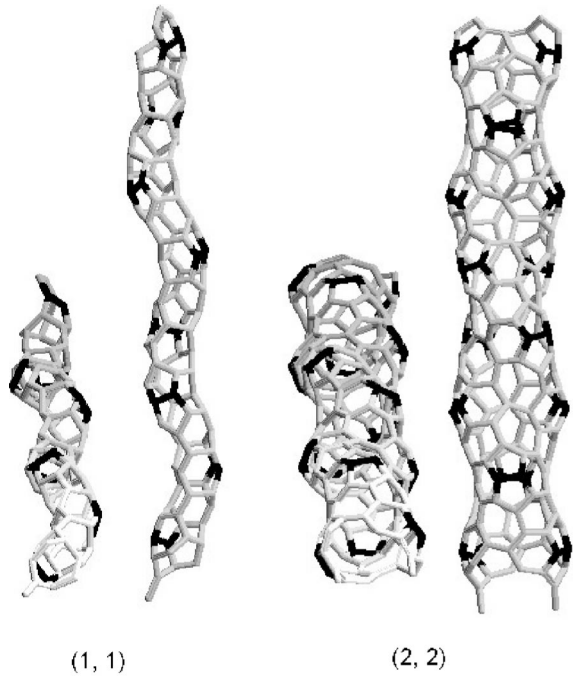


FIG. 3. Atomic structures of open-end nanotubes (1,1) and (2,2) viewed from two directions.

one finds four stripes spiraling around the tubular structure. On the other hand the pitch values and the left or right handedness are different for each object. An interesting feature worth pointing out for (4,0) is the occurrence of some of the highlighted bonds in cavities (negative stressor) so deep, that the two neighboring positive stressors on the sides of the cavity are almost at the same distance as the side by side positive stressors (Fig. 2, longitudinal view). While (4,4) is close to a circular section tube, which has some local protrusions, (0,4) is a necklace of pearls. The “pearls” are made by stressor rows that encircle the nanotube at regular intervals along the axis, with rings of heptagons between them where a negative curvature is realized. It is worth mentioning that the bonding energy per atom for this structure is  $-7.06$  eV, below that of the planar Haeckelite sheet of Fig. 1,  $-6.83$  eV, and close to the value for a graphene sheet,  $-7.37$  eV. Another interesting feature of this structure is that it can be easily amplified, i.e., by inserting additional polygons in the equatorial region, one may increase the size of the “pearls.”

A particular case of the  $(n,n)$ -type structures has to be mentioned: the (1,1) case. For this structure in any section of the 0.56-nm length of the tube, one finds zero or one positive stressor. This means that there is no stress compensation within the section and this will lead to the curling of the tube (curling is discussed previously in Ref. 26). For the (2,2) case, there will be zero or a multiple of two stressors in any section of the tube. The two stress concentrators are placed in such a way that they face each other, so that the stress is equilibrated and a somewhat flattened double helix is produced (Fig. 3), like the one discussed in Ref. 26.

The first three structures situated on the  $(n,0)$  axis are shown in Fig. 4: (1,0) is a nice coil similar to the one already

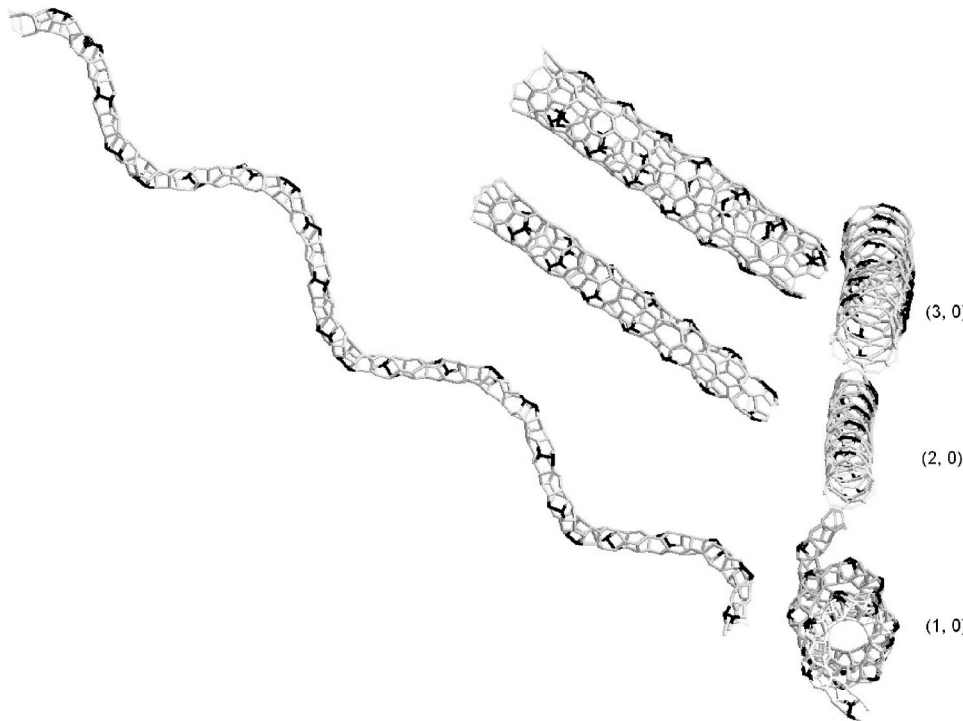


FIG. 4. Atomic structures of open-end nanotubes (1,0), (2,0), and (3,0) viewed from two directions.

discussed in our earlier paper.<sup>26</sup> Here again, the coiling is due to the asymmetric position of the single stressor within the unit cell. The structures (2,0) and (3,0) gain an increasingly circular section tube aspect with increasing  $n$ . Starting from the tube (4,0) shown in Fig. 2, the stress resulted from rolling the planar structure into a tube has decreased sufficiently to allow some of the stressors to occupy an inward position. For example, the tube (7,0) will have a structure in which both the dips and the protrusions spiral regularly along the tube. Apparently, there is a radius limit, around 0.5 nm, over which the stress due to the cylindrical curvature is low enough to allow inward dips for some stressors. However, not all tubular structures with a larger radius will show dips. While none of the structures that we investigated in detail shows dips below this radius, there are structures with a symmetric distribution of stressors around the wrapping vector, such as (4,4) or (2,6), Fig. 1(b), which have a larger radius than 0.5 nm and do not present dips. On the other hand the structures with an asymmetric distribution of stressors, such as (5,2) and (4,2), show dips. (4,3), next to (4,4), has a flattened out, twisted ribbonlike shape due to the dips.

The region between the  $(n,n)$  and the  $(n,0)$  axes contains tubular-type structures  $(n,m)$ , where  $n \neq m$  and  $n,m \neq 0$ , such as the ones shown in Fig. 5. The number of stressor stripes in the structure is equal to  $n \times m$ , however, not necessarily all stressors are “visible” when scanning along the tube axis. For example, in the case of structure (5,2), half of the stressors are situated in cavities. Figure 1(b) shows the stressor arrangement for this structure. The stressors which are not equilibrated by corresponding stressors on the other side are highlighted by encircling. There is an observation to be made: the stresses on the left- and right-hand sides of the wrapping vector are not equal; this will yield a mild curvature of the structure, which may be the indication of super-

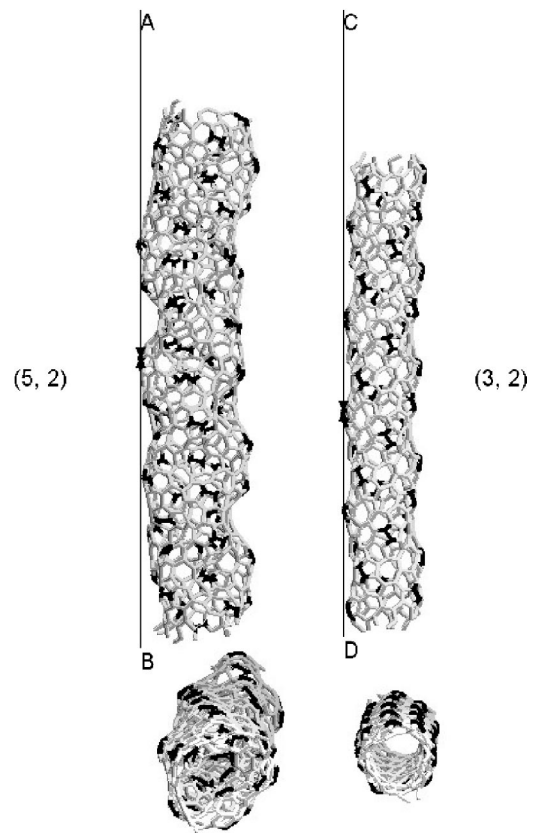


FIG. 5. Atomic structures of open-end nanotubes (5,2) and (3,2) viewed from two directions. The slight curling of the nanotube axis can be seen by referring to the thin vertical lines.

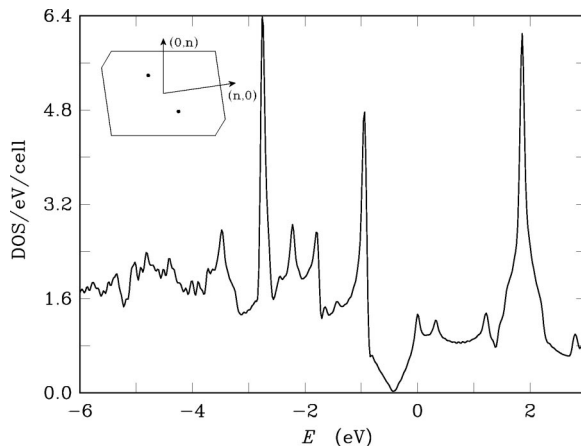


FIG. 6. Tight-binding  $\pi$  density of states of the two-dimensional Haeckelite network of Fig. 1 calculated with the hopping interaction  $\gamma_0 = -2.77$  eV (Ref. 28). The Fermi level is located in the zero gap at  $-0.43$  eV. The inset shows the first Brillouin zone of the Haeckelite plane, the two black circles are the Fermi points, and the arrows indicate the axial directions of the  $(n,0)$  and  $(0,n)$  nanotubes.

coiling with a very large radius of curvature. As shown in Fig. 5, the  $(3,2)$  tube also shows a mild curvature due to the nonsymmetrical distribution of the stressor around the wrapping vector such as for the  $(5,2)$  case, but here all stressors are visible on protrusions, so that six stressor stripes are visible parallel to the tube axis, and the individual stressors can be grouped in three spirals coiling around the tube. A similar arrangement of stressors is found for  $(2,6)$ , but the number of axial stripes is 12.

### III. ELECTRONIC PROPERTIES

The electronic densities of states of the Haeckelite nanotubes were computed with a tight-binding Slater-Koster Hamiltonian that incorporates the four  $2s$  and  $2p$  valence orbitals of C. The tight-binding hopping parameters used were taken from Ref. 28. In all the optimized structures, the bond lengths were found to lie in a narrow interval around 0.142 nm, of 2–4 pm width, typically. The corresponding strain of the bonds was accounted for by allowing the hopping parameters to vary according to a  $d^{-2}$  law. The effects of electron transfer from the heptagons to the pentagons were neglected. These charge transfers could have been treated self-consistently. However, this procedure was not undertaken because, to our best knowledge, there is no result from density-functional theory with which to compare. Instead, the electronic structures of Haeckelite structures<sup>25,29</sup> published so far were obtained with a tight-binding Hamiltonian similar to ours, without charge transfers. Only the nanotubes with a diameter larger than 0.6 nm were considered in this study, because the tight-binding Hamiltonian may not be accurate enough for carbon nanotubes with small diameters. The nanotubes are listed in Table I. Interestingly enough, all the nanotubes were found to be semiconductors. By comparison, the Haeckelite nanotubes of Ref. 25 were all metallic.

Here, the infinite, two-dimensional Haeckelite sheet having the flat structure of Fig. 1, from which the nanotubes

were rolled up, is a zero-gap semiconductor like graphene. The density of states of this structure, calculated with the  $\pi$  electrons only, is shown in Fig. 6. Because it is a planar structure, the  $\pi$  states do not couple to the  $\sigma$  states. The zero of energy is the energy of the C  $2p$  orbital. Two  $\pi$  bands cross each other at the Fermi energy located at  $E_F = -0.43$  eV. This crossing takes place at two points in the first Brillouin zone, symmetrically located with respect to the  $\Gamma$  point at a distance of  $0.25 \text{ \AA}^{-1}$  (see the inset of Fig. 6). Due to the absence of symmetry in the first Brillouin zone, almost all the nanotubes built from Fig. 1 will be semiconductors, because it is unlikely that the Fermi wave vector of the 2D sheet be an allowed wave vector of the nanotube when cyclic periodic conditions are imposed along the circumference, except for large diameters.

As illustrative examples, the densities of states of three nanotubes are shown in Fig. 7. For each tube, the solid-line curve is the density of states (DOS) computed with the Slater-Koster Hamiltonian, taking into account the bond strain as explained above. The DOS so obtained depends on the details of the geometry optimization. The positive and negative curvatures of the structure generated by the pentagons and heptagons is indeed responsible for a strong mixing between  $\pi$  and  $\sigma$  states. The effects of this mixing can be measured by comparing the four-electron DOS with the one obtained with the  $\pi$  electrons only, assuming further that the hopping parameter is independent of both the bond length and the relative orientation of the  $\pi$  orbitals. In so doing, a purely topological part of the DOS is determined. It is represented by the dashed-line curves in Fig. 7, which can be directly compared to the  $\pi$  DOS of the flat sheet shown in Fig. 6. This topological DOS is robust, since it is independent of the structural optimization. The  $\sigma$ - $\pi$  mixing clearly affects the density of states, even close to the Fermi level. By comparison with the topological gap, the band gap obtained by the Slater-Koster Hamiltonian is modified in position and width by a few tenths of an eV. However, the  $\sigma$ - $\pi$  mixing and the bond strain do not modify qualitatively the important result that the nanotubes all are semiconductors. The band gap, centered on  $E_F$ , is located slightly below the energy of the C  $2p$  orbital unlike the case of the semiconducting single-wall graphitic nanotubes where the gap is centered on the position of the  $2p$  orbital. Here, the presence of odd-membered rings destroys the electron-hole symmetry, which shifts the gap down. There is an effect of the wrapping indices of the width of the topological band gap, the overall rule being that increasing diameter decreases the gap (see Table I). The nanotube  $(5,2)$  is nearly metallic. It has a small band gap of about 0.1 eV, not totally formed due to a broadening function used in the DOS calculations, and which only appears as a dip near  $E = -0.45$  eV in the topological DOS of Fig. 7(c). All the nanotube densities of states shown in Fig. 7 present a peak at around  $-1$  eV that is already present in the  $\pi$  DOS of the 2D Haeckelite plane, Fig. 6.

### IV. COMPUTED STM IMAGES

It is difficult to obtain atomic resolution with the scanning-tunneling microscope on nanotubes grown by cata-

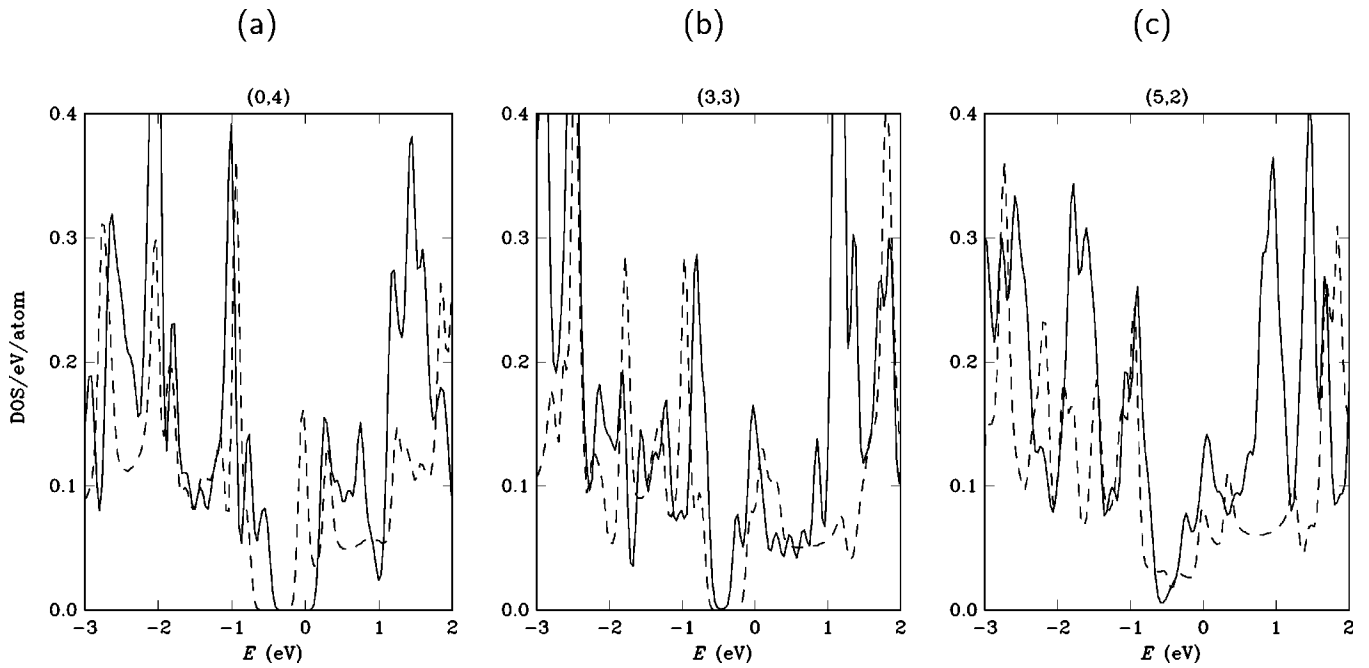


FIG. 7. Tight-binding  $\sigma + \pi$  (full line) and  $\pi$ -only (dashed line) densities of states of the nanotubes (0,4), (3,3), and (5,2) calculated with the Mintmire and White parameters (Ref.<sup>28</sup>). All the tubes are semiconductors. The zero of energy is the position of the C  $2p$  orbital.

lytic CVD.<sup>30</sup> It is a fact that these nanotubes are produced at lower temperature than that realized with laser ablation or arc discharge techniques. For that reason, the CVD nanotubes have probably more defects than the ones produced by the other, high-temperature techniques (see discussion below). It is therefore interesting to explore by computer simulation whether the atomic resolution of a nanotube can indeed be lost when a large number of defects are incorporated in the structure. The Haeckelite nanotubes are good candidates to deal with for that purpose.

Constant-current STM images of Haeckelite nanotubes were computed with a tight-binding formalism.<sup>31</sup> This formalism has been shown to agree fairly well with Tersoff-Hamann density-functional theory of STM in the case of perfect carbon nanotubes.<sup>32</sup> For the sake of simplicity, only the  $\pi$  orbitals of the nanotube were considered. This is justified because for the bias potential used, the density of states is dominated by the  $\pi$ -electron states. A general observation that can be made from these calculations is that the protruding stressors in the Haeckelite nanotubes give rise to maxima of tunneling current. This is a general property of the pentagonal defects in carbon nanotubes that gives rise to salient features in the STM images.<sup>33,34</sup> One clearly sees hillocks associated with the pentagon pairs in the STM image of (3,3) displayed in Fig. 8(a). This nanotube is characterized by three rows of positive stressors that spiral around the nanotube. The stressors do not protrude very much, 0.75 Å above the average radius of the nanotube. Nevertheless, they give rise to remarkable corrugation in the STM image. Although only the topmost section of the nanotube is seen in the computed STM image, still it is possible to identify rows of stressors from the bright features, oriented at 38° with respect to the tube axis and spiraling around the structure.

In a similar way the positive stressors generate maxima

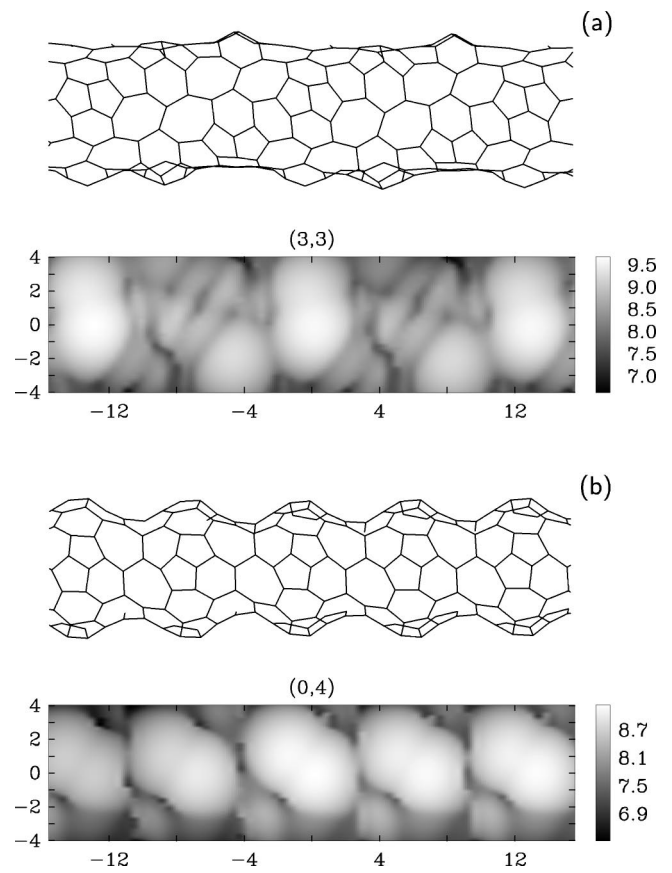


FIG. 8. Computed STM images of two Haeckelite nanotubes with indices (a) (3,3) and (b) (0,4). A top view of the atomic structure is displayed above the STM image, both with the same scale along the axial direction. The Fermi level of the tip is 0.1-eV above the C  $2p$  atomic orbital (which corresponds to +0.1 eV in the density of states represented by dashed lines in Fig. 7).

for the pearl-necklace-like (0,4) nanotube shown in Fig. 8(b). Regularly spaced hillocks of protrusions are clearly seen, with an elongated shape oriented parallel to the stressors. They are separated by sharp dips associated with the heptagons.

Another remarkable characteristic of the computed STM images is that it is impossible to recognize the atomic structure of the Haeckelite nanotubes from the topography. The number of pentagons and heptagons is so large that the electronic density of states is deeply perturbed. The perturbation is not evenly distributed on the atoms, so that the imaged atomic structure is strongly deformed by the electronic effects. This observation confirms recent calculations of the STM image of zigzag and armchair nanotube tapers where a series of pentagon-heptagon pairs masks the underlying atomic structure.<sup>35</sup>

## V. DISCUSSION

As is well known, the multiwall carbon nanotubes (MWCNTs) grown by various low-temperature methods, usually based on the use of some kind of catalytic process and low growth temperatures in the range of 600°–800°C, frequently present random curvature. This is clearly opposite to the arc grown MWCNTs, which usually are straight, although, under certain special conditions, these tubes may exhibit knees and branching but they remain straight between these well-localized modifications in structure. A quantitative investigation by x-ray diffraction, TEM, and electron microdiffraction of the defect removal by thermal annealing up to 3000°C of catalytically produced MWCNTs showed that the interlayer spacing of as-grown tubes may be as large as  $d_{ONT(200)} = 0.342\ 35\ \text{nm}$ , and this spacing decreases after the highest-temperature annealing to  $d_{NT(200)} = 0.339\ 82\ \text{nm}$ .<sup>36</sup> Parallel to the reduction of the interlayer spacing, the electron-diffraction pattern shows the increase of graphitic ordering. Indeed, the HRTEM images of catalytically grown nanotubes taken in an as-grown state may show from mild<sup>37</sup> to strong<sup>38</sup> crumbling of the layers constituting the tube. The global morphology of the grown nanotubes is heavily influenced by the growth temperature in the range 550°C–850°C;<sup>38</sup> the lower the growth temperature, the more curved the tubes. Although the HRTEM images do not readily identify the kind of defects, it is reasonable to accept that the crumbling of the perfect graphene sheets and the curved shape of the nanotubes are caused by the incorporation of nonhexagonal rings.

Atomic resolution STM images and STS spectra showed that even in the case of single-wall nanotubes grown by laser ablation, for which a growth temperature over 2000°C may be assumed, 10% of the nanotubes may incorporate nonhexagonal rings.<sup>17</sup> This is a very strong argument for the fact that the nanotubes grown at much lower temperatures can contain a much larger fraction of nonhexagonal rings.

When a catalytic nanotube starts growing, the first step is the encapsulation of the catalyst particle by graphiticlike layers. Since most catalyst particles have rounded shapes, especially in the melt or premelt state, this can be achieved only if some nonhexagonal rings are incorporated in the graphitic

sheet. Most frequently the nonhexagonal rings are incorporated randomly, and randomly curved tubes are produced. However, under specific conditions such as those used in Refs. 3, 20, and 21, a particular combination of hexagonal and nonhexagonal rings may be achieved, which has a stability comparable to that of graphene, see Table I. At the low growth temperatures used in the catalytic process, such a combination may not anneal out, when the growing layer(s) separate from the catalytic particle. Then the addition of new carbon atoms to the growing tube has to match the structure of the already grown layer(s) to achieve the energy minimum.

A justified question is why in the single-wall carbon nanotubes grown by the catalytic procedure no regularly coiled carbon nanotubes found? As the data of Ref. 3 show, the growth temperature has a strong influence on the morphology of the grown tubes even if all other parameters are kept constant. Similar findings were reported for the case of coiled carbon filaments,<sup>39</sup> which have a thickness in the range of several hundreds of nanometers. A very narrow temperature range from 740°C to 820°C was found in those regular coils that were produced. It is worth pointing out that for the case of vapor-grown graphitic filaments, it was shown that the backbone of the filament is a carbon nanotube, over which amorphous carbon is deposited.<sup>40,41</sup> It is then justified to assume that in the case of the regular coils reported in Ref. 39, the core of the growing coil may be a nanotube, too. Taking into account that the single-wall carbon nanotubes grown by the catalytic method are produced in the range of temperatures around 1000°C, it is unlikely to find coiled tubes at this temperature. On the other hand, single-wall, tightly wound carbon nanotube coils have been found by STM in catalytic tubes grown at 700°C by the decomposition of acetylene over a Co catalyst.<sup>42</sup> Coiled and branched carbon nanotubes were grown on graphite substrates at room temperature by a different method: the deposition of carbon clusters resulted from C<sub>60</sub> decomposition.<sup>10</sup> However, in this experiment the growth does not take place on catalyst particles, but the fullerene fragments may take a conformation which will promote the growth of coiled tubes.

One of the structures with the stability close to that of graphene is the necklace of pearls (0,4). It should be pointed out that the increase of  $n$  for these (0, $n$ )-type structures results in the increase of diameter of the “pearl,” while the periodicity of the object is conserved due to the way in which the heptagonal rows are arranged in the sheet shown in Fig. 1. This means that the necklaces of pearls can be easily generated as multishell objects. As a matter of fact, in a recent paper,<sup>43</sup> Jourdain *et al.* describe pearl-shaped regions on catalytically grown carbon nanotubes. It is remarkable that according to their growth mechanism, the catalyst particle is in a molten state during the growth, so that its shape cannot determine the shape of the pearl, but the successive pearls still show similarity in shape. In contrast to their pearls which contain encapsulated catalysts, similar structures have been reported by Blank *et al.*,<sup>44</sup> which are made of a succession of empty, roughly spherically shaped “pearls.” The authors called these structures “surface modulated spherical layer nanotubes” (see Fig. 7 in Ref. 44).

These types of nanotubes were observed when the carbon vapor was generated using a mixture of  $C_{60}$  and Fe. The HRTEM images clearly show that the walls of the pearls are constituted from slightly crumpled sheets, contrary to other carbon nanostructures produced in the same installation, which have straight, well-graphitized walls (see Fig. 6 in Ref. 44). We may identify these crumpled sheets with Haeckelite sheets.

The Haeckelite  $57\text{-}3\times6$ -type plane itself, Fig. 1, is a stable structure which, if allowed to relax freely in three dimensions will transform into a crumpled sheet that has a binding energy of  $-7.05$  eV/atom, close to that of graphene. The crumpling is caused by the relaxation of stress introduced by the stressors. On the other hand the structure does not have to be perturbed by inserting into it polygons which are not “naturally” incorporated. This means that when a structure such as that formed by wrapping such a sheet (as discussed earlier in this paper) grows in low-temperature conditions, with low mobility of adatoms and possibly on a spherically shaped molten or solid catalytic particle—the curvature of which selected a particular Haeckelite sheet from the multitude of possible arrangements—it is more likely that the newly arriving carbon atoms will be incorporated in a way determined by the structure of the sheet more than any other way, including the atomic arrangement corresponding to a graphene sheet. This is a mechanism that can explain the question that previously did not have a satisfactory answer: why are some of the experimentally produced coils so regularly coiled? Although structurally correct, the previous models did not elucidate which mechanism facilitates the regular switching back and forth from the formation of a perfect graphitic network and the local incorporation of pentagons or heptagons.

We believe that the above results may prove useful for the interpretation of the experimental data. For example, the STM image of the coil in Fig. 5(a) of Ref. 10 is clearly a single-strand coil, but the object shown in Fig. 5(b) was interpreted to be a double-strand coil in a similar way to the multiple coils reported in Refs. 20 and 21. As long as such objects are rarely found, one may accept the accidental inter-coiling of two identical pitch coils. However, when such objects can be produced on a regular basis, it is difficult to propose a mechanism which would be responsible for the systematic production of multistrand coils with identical pitch values. It seems reasonable to identify these multi-strand objects with Haeckelite-type tubes produced under the specific growth conditions used.

When the growth takes place at higher temperatures, the mobility of adatoms and even the mobility due to the thermal energy of the already incorporated carbon atoms is high enough—as shown by the annealing experiments carried out by Andrews *et al.*<sup>36</sup>—to allow jumping over the energy barrier which separates a certain Haeckelite-type sheet from the slightly more stable graphene sheet. Therefore in the arc and the laser ablation grown nanotubes only isolated defects are found, whereas the catalytically grown nanotubes may be

fully constituted of Haeckelite tubes, or in the case of randomly curved tubes, from pieces of different Haeckelite structures.

The Haeckelite  $57\text{-}3\times6$  sheet discussed in the present paper is just one of the many possible ones, yet it generates a very rich variety of shapes. It is reasonable to assume that by starting from different sheets it is possible to build multiple shell structures, such as the ones more frequently observed experimentally.<sup>3,20,21</sup>

## VI. CONCLUSIONS

A family of Haeckelite-type, tubular carbon nanostructures with complex shapes was generated using a similar formalism to the one usually applied for the generation of straight, graphitic carbon nanotubes. The stability of the fully relaxed  $57\text{-}3\times6$ -type sheet was found to be close to that of a graphene plane. The structures are constructed by rolling up a perfect, threefold coordinated carbon network built from two azulene units (fused 5–7 rings) and three hexagons. The bond joining the two adjacent pentagons was found to be a stress concentrator of the structure, which we call a stressor. The shape the tubular structures take after energy minimization using the Brenner-Tersoff potential is strongly influenced by the way in which the stressors are placed in the unit cell. A large variety of stable structures was constructed: single and multistrand coils; straight, circular section tubes on which multiple stressor stripes spiral along the axis, producing both topographic features and STM current maxima; pearl-necklace-type structures with a very high degree of stability and from which one can easily build multishell structures, etc. Most frequently the structures investigated in detail are semiconductors with a gap of approximately 0.6 eV, and sometimes nearly metallic structures are found too, such as the (4,0) and (5,2) nanotubes (see Table I).

The STM images calculated using a tight-binding formalism showed that due to the large number of nonhexagonal rings, no atomic resolution is to be expected on Haeckelite-type tubular structures, and the positive stressors are associated with tunneling current maxima.

By comparing our constructions to experimental results of some unusual-looking carbon nanostructures, we tentatively identified some of the double- and triple-strand coiled tubes, and the pearl-necklace-like structures with possible structural models of those recently reported carbon nano-objects.<sup>21,43</sup>

## ACKNOWLEDGMENTS

This work has been partly funded by the IUAP research Project No. P5/01 on “Quantum Size Effects in Nanostructured Materials” of the Belgian Office for Scientific, Technical, and Cultural Affairs. It has been supported by the EU in the frame of a Center of Excellence project under Contract No. ICA1-CT-2000-70029. This work has also benefitted from financial support from the Belgian FNRS and the Hungarian Academy of Sciences and by Hungarian OTKA Grant No. T043685.

- <sup>1</sup>D. Ugarte, Nature (London) **359**, 707 (1992).
- <sup>2</sup>F. Le Normand, L. Constant, G. Ehret, and C. Speisser, J. Mater. Res. **14**, 560 (1999).
- <sup>3</sup>S. Amelinckx, X.B. Zhang, D. Bernaerts, X.F. Zhang, V. Ivanov, and J. B.Nagy, Science (Washington, DC, U.S.) **265**, 635 (1994).
- <sup>4</sup>J. Liu, H. Dai, J.H. Hafner, D.T. Colbert, R.E. Smalley, S.J. Tans, and C. Dekker, Nature (London) **385**, 780 (1997).
- <sup>5</sup>M. Sano, A. Kamino, J. Okamura, and S. Shinkai, Science (Washington, DC, U.S.) **293**, 1299 (2001).
- <sup>6</sup>A. Krishnan, E. Dujardin, M.M.J. Treacy, J. Hugdahl, S. Lynum, and T.W. Ebbesen, Nature (London) **388**, 451 (1997).
- <sup>7</sup>S. Iijima, M. Yudasaka, R. Yamada, S. Bandow, K. Suenaga, F. Kokai, and K. Takahashi, Chem. Phys. Lett. **309**, 165 (1999).
- <sup>8</sup>J. Li, Ch. Papadopoulos, and J. Xu, Nature (London) **402**, 253 (1999).
- <sup>9</sup>P. Nagy, R. Ehlich, L.P. Biró, and J. Gyulai, Appl. Phys. A: Mater. Sci. Process. **70**, 481 (2000).
- <sup>10</sup>L.P. Biró, R. Ehlich, Z. Osváth, A. Koós, Z.E. Horváth, J. Gyulai, and J. B.Nagy, Mater. Sci. Eng., C **C19**, 3 (2002).
- <sup>11</sup>M. Terrones, W.K. Hsu, J.P. Hare, H.W. Kroto, H. Terrones, and D.R.M. Walton, Philos. Trans. R. Soc. London, Ser. A **354**, 2025 (1996).
- <sup>12</sup>S. Iijima, T. Ichihashi, and Y. Ando, Nature (London) **356**, 776 (1992).
- <sup>13</sup>D.N. Weldon, W.J. Blau, and H.W. Zandbergen, Chem. Phys. Lett. **241**, 365 (1995).
- <sup>14</sup>G.E. Scuseria, Chem. Phys. Lett. **195**, 534 (1992).
- <sup>15</sup>M. Terrones, F. Banhart, N. Grobert, J.C. Charlier, H. Terrones, and P.M. Ajayan, Phys. Rev. Lett. **89**, 075505 (2002).
- <sup>16</sup>B.I. Dunlap, Phys. Rev. B **46**, 1933 (1992).
- <sup>17</sup>M. Ouyang, J.L. Huang, and C.M. Lieber, Science (Washington, DC, U.S.) **291**, 97 (2001).
- <sup>18</sup>M. Monthioux, Carbon **40**, 1809 (2002).
- <sup>19</sup>S. Ihara, S. Itoh, and J.I. Kitakami, Phys. Rev. B **48**, 5643 (1993).
- <sup>20</sup>M. Zhang, Y. Nakayama, and L. Pan, Jpn. J. Appl. Phys., Part 2 **39**, L1242 (2000).
- <sup>21</sup>C.J. Su, D.W. Hwang, S.H. Lin, B.Y. Jin, and L.P. Hwang, Phys. Chem. Comm. **5**, 34 (2002).
- <sup>22</sup>I. László and A. Rassat, Int. J. Quantum Chem. **84**, 136 (2001).
- <sup>23</sup>J. Berger and J.E. Avron, J. Chem. Soc., Faraday Trans. **91**, 4037 (1995).
- <sup>24</sup>I. László, A. Rassat, P.W. Fowler, and A. Graovac, Chem. Phys. Lett. **342**, 369 (2001).
- <sup>25</sup>H. Terrones, M. Terrones, E. Hernandez, N. Grobert, J.C. Charlier, and P.M. Ajayan, Phys. Rev. Lett. **84**, 1716 (2000).
- <sup>26</sup>L.P. Biró, G.I. Márk, A.A. Koós, J.B. Nagy, and Ph. Lambin, Phys. Rev. B **66**, 165405 (2002).
- <sup>27</sup>M.S. Dresselhaus, G. Dresselhaus, and P.C. Eklund, *Science of Fullerenes and Carbon Nanotubes* (Academic, San Diego, 1996).
- <sup>28</sup>J.W. Mintmire and C.T. White, Carbon **33**, 893 (1995).
- <sup>29</sup>V.H. Crespi, L.X. Benedict, M.L. Cohen, and S.G. Louie, Phys. Rev. B **53**, R13 303 (1996).
- <sup>30</sup>L.P. Biró, J. Gyulai, Ph. Lambin, J.B. Nagy, S. Lazarescu, G.I. Márk, A. Fonseca, P.R. Surján, Zs. Szekeres, P.A. Thiry, and A.A. Lucas, Carbon **36**, 689 (1998).
- <sup>31</sup>V. Meunier and Ph. Lambin, Phys. Rev. Lett. **81**, 5888 (1998).
- <sup>32</sup>A. Rubio, Appl. Phys. A: Mater. Sci. Process. **68**, 275 (1999).
- <sup>33</sup>V. Meunier and Ph. Lambin, Carbon **38**, 1729 (2000).
- <sup>34</sup>D. Orlikowski, M. Buongiorno Nardelli, J. Bernholc, and Ch. Roland, Phys. Rev. B **61**, 14 194 (2000).
- <sup>35</sup>V. Meunier, M. Buongiorno Nardelli, C. Roland, and J. Bernholc, Phys. Rev. B **64**, 195419 (2001).
- <sup>36</sup>R. Andrews, D. Jacques, D. Qian, and E.C. Dickey, Carbon **39**, 1681 (2001).
- <sup>37</sup>M. Chhowalla, K.B.K. Teo, C. Ducati, N.L. Rupasinghe, G.A.J. Amaralunga, A.C. Ferrari, D. Roy, J. Robertson, and W.I. Milne, J. Appl. Phys. **90**, 5308 (2001).
- <sup>38</sup>C. Ducati, I. Alexandrou, M. Chhowalla, G.A.J. Amaralunga, and J. Robertson, Appl. Phys. Lett. **92**, 3299 (2002).
- <sup>39</sup>X. Chen and S. Motojima, Carbon **37**, 1817 (1999).
- <sup>40</sup>M. Endo, K. Takeuchi, K. Kobori, K. Takahashi, H.W. Kroto, and A. Sarkar, Carbon **33**, 873 (1995).
- <sup>41</sup>Ph. Serp and J.L. Figueiredo, Carbon **35**, 675 (1997).
- <sup>42</sup>L.P. Biró, S.D. Lazarescu, P.A. Thiry, A. Fonseca, J. B.Nagy, A.A. Lucas, and Ph. Lambin, Europhys. Lett. **50**, 494 (2000).
- <sup>43</sup>V. Jourdain, H. Kanzow, M. Castignolles, A. Loiseau, and P. Bernier, Chem. Phys. Lett. **364**, 27 (2002).
- <sup>44</sup>V.D. Blank, I.G. Gorlova, J.L. Hutchison, N.A. Kiselev, A.B. Ormont, E.V. Polyakov, J. Sloan, D.N. Zakharov, and S.G. Zybtsev, Carbon **38**, 1217 (2000).